Progress In Electromagnetics Research B, Vol. 56, 387–407, 2013

FOCUSING PROPERTIES OF ULTRA WIDEBAND TRANSIENT ARRAYS

Shaya Karimkashi[1, *], Ahmed A. Kishk[2], Darko Kajfez[3], and Guifu Zhang[1]

[1]Advanced Radar Research Center, University of Oklahoma, 120 David L. Boren Blvd. Ste. 4600, National Weather Center, Norman, OK 73072-7307, USA

[2]Department of Electrical and Computer Engineering, Concordia University, 1455 De Maisonneuve Blvd. West, EV 005.139, Montreal, QC, H3G 1M8, Canada

[3]Electrical Engineering Department, University of Mississippi, Anderson Hall Room 312, University, MS 38677, USA

Abstract—Some new focusing properties of time-domain ultra wide band (UWB) focusing array antennas are presented. The large current radiator (LCR) is considered as the UWB antenna element. Each LCR is replaced by a set of infinitesimal dipoles modeling both the near field and the far field patterns of the antenna element, as well as the coupling between the elements. Several antenna arrays with different sizes and numbers of elements are modeled. It is shown that similar to narrow band antennas, the actual maximum field region shifts from the intended focus region towards the antenna aperture.

1. INTRODUCTION

Focusing the microwave energy of an antenna into small regions can be accomplished by using focused antennas where the microwave power is targeted at a point close to the antenna aperture. Different antennas including arrays, reflectors, and dielectric lens antennas as well as Fresnel zone plate antennas have been used for this purpose [1–7]. Focused array antennas based on Ultra-Wide-Band (UWB) impulse waveforms can highly concentrate electromagnetic energy into small regions by controlling the timing of pulses radiated by each element [8–16]. Better performance compared to narrowband arrays can be

Received 6 August 2013, Accepted 5 November 2013, Scheduled 14 November 2013

* Corresponding author: Shaya Karimkashi (shaya.karimkashi@ou.edu).

achieved in terms of higher angular resolution and increasing the peak power delivered to the focused region. These antennas are of interest in medical applications, radar, homeland security systems and communication systems [3, 9–12, 17–22]. The performance of the focused array can be further improved by increasing the number of elements [9] or element spacing [19, 23–26]. However, increasing both the number of elements and the spacing between elements produces a larger aperture array. Using thinned arrays, higher performance with a fewer number of elements with the same aperture size can be obtained [15, 27]. In addition, sparse focused array antennas are used to achieve better performance for the focused antennas [19, 28].

The main goal of this paper is to study some focusing and defocusing behavior of time-domain UWB focused arrays. The Large Current Radiator (LCR) is considered as the array element. Figure 1 shows the configuration of an LCR, consisting of a generator, a closed loop and a ferrite plate. The LCR is inherently a non-resonating structure and can thus radiate electromagnetic (EM) waves with either sinusoidal or non-sinusoidal time variation [29–33]. In order to model the mutual coupling between the LCR elements within the array, the infinitesimal dipole array modeling is considered. Using this method, each LCR is replaced by a set of infinitesimal dipoles producing the same electromagnetic fields as the LCR.

The concept of infinitesimal dipole moments (IDM) was first introduced in [34] for modeling the near field of radiating structures in biomedical applications. The idea was formulated in [35–38] to find sets of infinitesimal dipoles by using a genetic algorithm. Later, the concept

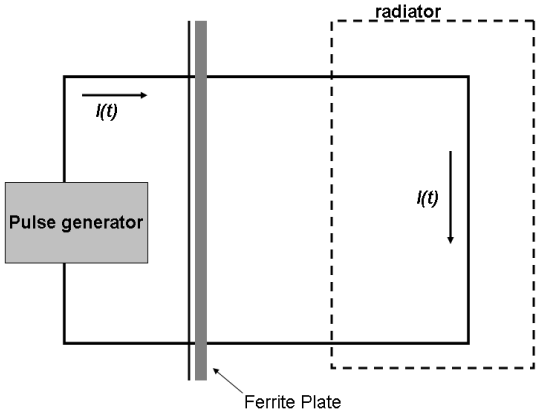

Figure 1. The schematic of an LCR.

was extended by applying quantum particle swarm optimization to the problem, and a method of predicting the mutual coupling between antenna elements was proposed [39]. In [40, 41] IDMs for dielectric resonators in multi-layer structures is obtained by using the particle swarm optimization method. In [42] a procedure of getting IDMs for wideband antennas was proposed and applied for a wideband stacked dielectric resonator antenna. The applications of IDMs for modeling and optimizing the array antennas are presented in [43, 44].

In this paper, the mutual coupling between the LCR elements is obtained using the reaction theorem [43–45]. It should be noted that LCR elements can be spaced at distances larger than the spatial duration of the pulse so that there aren't mutual coupling and multiple scattering effects between the elements. However, using the IDMs concept, the array can be modeled by assuming any spacing between the elements. Using this method, several antenna arrays and the coupling between their elements will be modeled.

This paper is organized as follows. In Section 2, the large current radiator modeling is presented. The infinitesimal dipole modeling for the array is demonstrated in Section 3. Section 4 investigates the focusing properties of uniformly spaced time domain array antennas. The conclusion is provided in Section 5.

2. LARGE CURRENT RADIATOR

2.1. LCR Modeling

The Large Current Radiator (LCR), which is one of the promising UWB radiators, was proposed by Harmuth [46–48]. This radiator is named Large Current Radiator because it is possible to create a large amplitude current in the radiating element with a relatively small driving voltage. Principally the LCR is a segment of a line conductor through which a current pulse of short duration but large amplitude is driven. Figure 2 shows the dimension of the chosen LCR. In order to model the LCR with the ferrite plate, only the radiator part of Figure 1 is modeled while the backward radiation is ignored because of the presence of the ferrite plate. The antenna is modeled in the frequency domain using a method of moment (MoM) based software (FEKO) [46] for the frequency range from 50 MHz to 3 GHz, and the time-domain radiated pattern is computed by using the inverse Fourier transform. The time-domain pattern, $F\ (\theta,\ \varphi,\ t,\ r)$, can be shown at certain time instances ($t = t_0$), distances ($r = r_0$) from the aperture, or observation angles ($\theta = \theta_0,\ \varphi = \varphi_0$).

The LCR is excited by a step voltage pulse with amplitude of 1 V and duration of 5.4 ns as shown in Figure 3(a). The radiated field

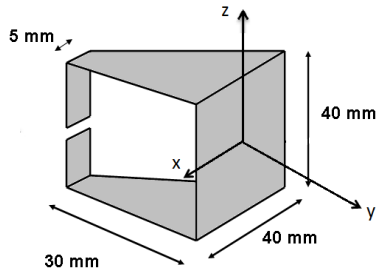

Figure 2. The configuration of modeled LCR.

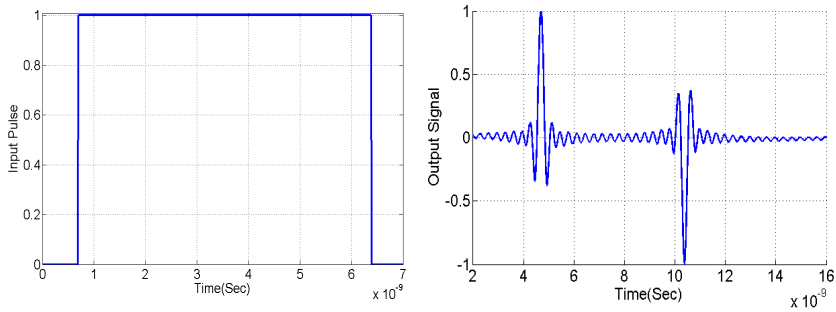

Figure 3. Time variation of (a) input voltage step pulse, and (b) pulse radiated by the large current radiator at broadside observation angles ($\theta = 90°$, $\varphi = 90°$) and a distance of $r = 1.2$ m from the antenna.

by the LCR at a distance of $y = 1.2\,\mathrm{m}$ from the antenna is shown in Figure 3(b). The time-domain near-field pattern of the LCR at the distance of $r = 1.2\,\mathrm{m}$ from the antenna in both E- and H-planes are shown in Figure 4.

In another effort, the LCR is excited by a Gaussian pulse $G(t)$ with different variances.

$$G(t) = \frac{1}{\sqrt{2\pi\sigma^2}} e^{-(t-u)^2/2\sigma^2} \tag{1}$$

where σ is the standard deviation and u is the mean. The advantage of the Gaussian pulse over the step pulse is that it has a limited bandwidth. The input Gaussian pulses in time domain and frequency domain are shown in Figures 5(a) and 5(b), respectively. The radiated pulses at the distance $y = 1.2\,\mathrm{m}$ from the LCR antenna in time domain and frequency domain are shown in Figures 5(c) and 5(d), respectively.

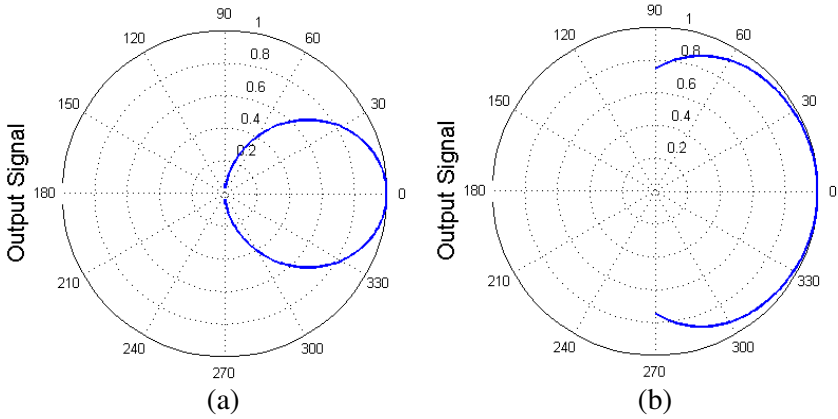

Figure 4. Time-domain near-field pattern of the LCR at the time instance of $t = 1.2/c$, and the distance of $r = 1.2\,\text{m}$ from the antenna aperture in the (a) E-plane and (b) H-plane.

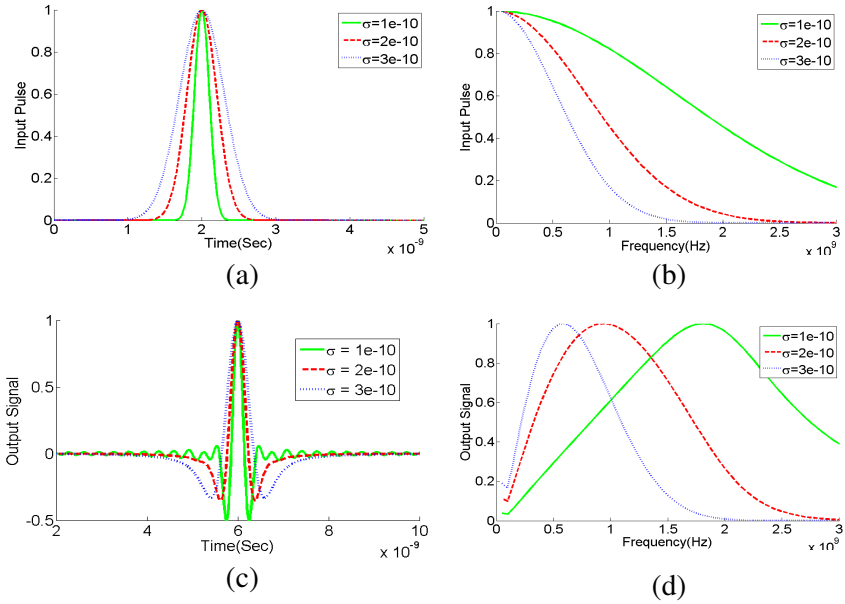

Figure 5. Input Gaussian pulse in the (a) time-domain and (b) in the frequency domain. Pulse radiated by the LCR at broadside observation angles ($\theta = 90^\circ$, $\varphi = 90^\circ$) and a distance of $r = 1.2\,\text{m}$ from the antenna. (c) Time-domain and (d) frequency domain.

It can be seen that the radiated pulses in Figure 5(c) have much less ringing variations compared to the one at Figure 3(b). By increasing the standard deviation, the number of sidelobes is decreased and a clear shaped pulse is created in the time domain. When the LCR is excited by a Gaussian pulse, the near field pattern at the time instance, $t = 1.2/c$, and a distance, $r = 1.2\,\mathrm{m}$, from the antenna aperture is shown in Figure 6. It can be seen that the near field patterns are very similar when the LCR is excited by step pulse or Gaussian pulse.

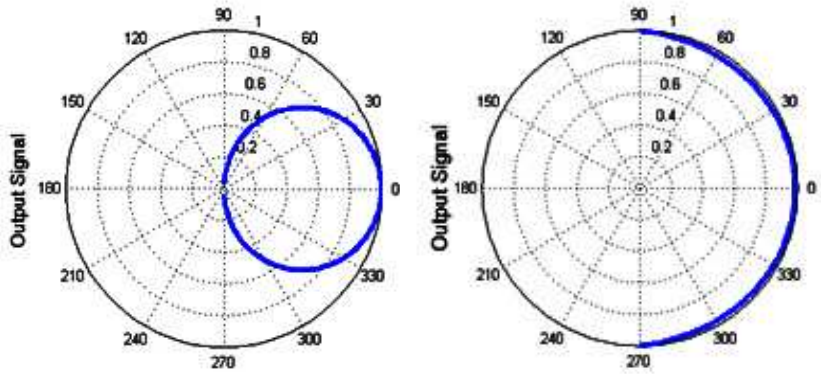

(a) (b)

Figure 6. Time-domain near-field pattern of the LCR at the time instance of $t = 1.2/c$ and a distance of $r = 1.2\,\mathrm{m}$ from the antenna aperture in the (a) E-plane and (b) H-plane.

2.2. Suppression of Mutual Coupling Effects by Increasing the Distance between Elements

It has been shown that LCR elements can be employed to achieve antenna arrays with high efficiencies [23, 28]. This can be done by spacing the LCRs at a distance much larger than the spatial duration of the radiated field pulse. In this case, there is no coupling between elements and the array antenna pattern can be obtained by the summation of each element pattern. In order to show the accuracy of this method, two LCRs spaced at a distance $d = 0.6\,\mathrm{m}$ are considered. One of the elements is excited by a step pulse and the other one is terminated to a matched load. Figure 7 shows the near field patterns of this configuration at both E- and H-planes compared to the near field patterns of one LCR element. It can be seen that very similar patterns are obtained for both planes. In other words, the presence of

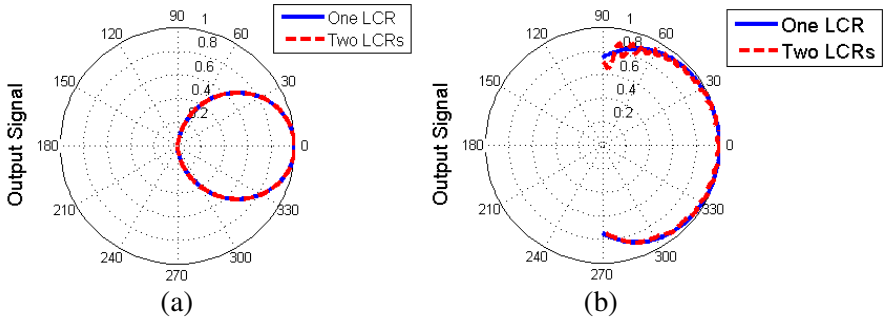

Figure 7. Comparison between the near field patterns of one-LCR and two-LCR element arrays at the time instance of $t = 1.2/c$ and a distance of $r = 1.2\,\text{m}$ from the antenna aperture in the (a) E-plane and (b) H-plane.

the loaded antenna at a distance larger than the spatial duration of the radiated pulse doesn't affect the radiation pattern of the LCR.

3. INFINITESIMAL DIPOLE MODELING

3.1. Methodology

A set of infinitesimal dipoles (electric or magnetic), representing an actual antenna, can be obtained by using an optimization algorithm to minimize the difference between the near field of the dipoles and those of the actual antenna. Each dipole is represented by seven parameters: the position of the elements (x, y, z coordinates); the complex dipole moment (the real and imaginary part), and its orientation (θ and φ). It should be mentioned that the dipole locations are limited within the volume of the actual antenna. Although electric dipoles, magnetic dipoles, or a combination of them can be used, we use only electric dipoles to represent the antenna [40].

In this algorithm, the IDM can be achieved by minimizing the error of the near field data defined as

$$e = \sum_{m=1}^{M_0} \sqrt{\frac{1}{3} \sum_{n=1}^{N_o} \left| \frac{\vec{E}_a(r_n, f_m)}{P_a} - \frac{\vec{E}_d(r_n, f_m)}{P_d} \right|^2} \tag{2}$$

where N_o and M_o are the number of observation points and frequency points, respectively. $\vec{E}_a(r_n, f_m)$ and $\vec{E}_d(r_n, f_m)$ are the electric fields on the observation surfaces, obtained by a full wave solution (FEKO) or measurements, and the electric dipoles, respectively. The vector r_n

is the position vector of the nth sampling point, f_m is the frequency and P is the maximum value of the electric field used for normalization as

$$P_{a,d} = \text{Max}\left\{\left|\vec{E}_{a,d}(r_n, f_m)\right|\right\}. \tag{3}$$

The subscript a is used to denote the measured or accurate solution obtained for the actual problem, and the subscript d is used to denote the desired solution obtained by the IDM model. It should be noted that in (2) the near field data are normalized. This is because the IDM is used to obtain the normalized spatial distribution of the near field, but not the real values that depend on the excitation amplitude of the antenna. The real field values due to the excitation of V_0 can be achieved by multiplying all the dipole moments with a factor of $V_0 P_a / P_d$ [39].

3.2. LCR and Its Infinitesimal Dipole Model

The LCR introduced in Section 2 is considered. The near-field is computed on a square observation plane with side lengths of 1000 mm located at a distance 500 mm from the antenna aperture. The near field is computed at 60 frequency points from 50 MHz to 3 GHz. The total number of samples is 121 points at each frequency. The modified invasive weed optimization (IWO) algorithm with restricted boundary condition is applied to determine the moment, the position, and the orientation of the dipoles. The total number of 30 electric dipoles is obtained after the optimization. The moments, locations and orientations of dipoles are shown in Table 1. The electric field

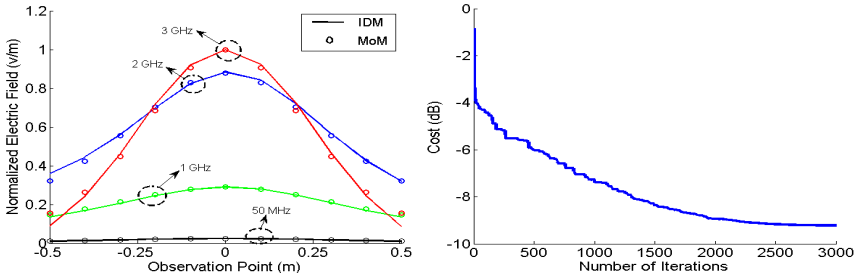

Figure 8. The optimized dipoles equivalent to the LCR. (a) Comparison of the electric field components of the near fields due to the actual antenna and IDMs over lines passing through the middle of the observation plane, and (b) the convergence curve of the IWO.

Table 1. The moments, positions and orientations of electric dipoles equivalent to LCR.

n_e	The dipole moment		The position of dipole (mm)			The orientation of dipole (degrees)	
	Re.	Im.	X	Y	Z	θ	Φ
1	−9.06	1.19	19.89	−19.99	−21.88	112.63	239.42
2	3.76	−0.22	5.97	−0.13	−27.95	23.97	242.16
3	−4.82	−3.65	9.82	5.32	−25.35	138.35	157.90
4	−7.98	−2.64	4.40	−11.55	−17.66	32.49	110.24
5	−9.97	−6.60	−11.38	−8.62	−10.92	174.85	259.74
6	4.97	−9.46	−7.34	−1.58	−5.10	74.82	275.18
7	7.63	0.84	6.20	7.58	−8.87	55.39	260.80
8	−9.94	1.09	18.56	17.05	−18.67	79.64	320.77
9	−1.02	−6.79	−3.62	−1.37	−10.24	65.30	320.38
10	−5.13	5.75	−19.99	6.73	−29.58	108.75	280.00
11	−6.17	−6.41	−1.58	−7.57	−17.34	170.72	290.79
12	−9.44	6.13	−19.99	−2.03	−15.49	88.84	226.77
13	1.36	7.18	12.83	8.59	−14.53	174.06	296.97
14	5.41	9.57	5.78	16.98	−29.99	43.67	273.48
15	−1.09	−2.25	−14.12	−0.16	−12.34	15.53	231.54
16	1.76	9.16	−10.26	−8.21	−10.30	122.64	3.47
17	−9.03	−3.99	−7.24	8.58	−13.78	76.00	219.89
18	−0.96	4.82	20.00	−0.60	−27.36	98.59	277.40
19	7.76	−4.99	−19.27	−13.93	−8.64	98.38	140.27
20	−0.84	−8.64	−5.78	14.34	−8.39	49.60	335.47
21	6.01	4.48	−5.29	−5.53	−29.17	99.50	245.04
22	−9.61	−7.46	0.21	−4.03	−29.99	61.59	82.82
23	0.98	−2.09	−19.13	3.45	−8.50	31.63	93.30
24	9.62	5.65	11.09	−12.51	−16.29	143.32	100.75
25	−0.38	0.99	8.06	19.72	−18.46	3.44	111.36
26	−6.38	7.93	8.59	16.93	−8.98	26.60	35.00
27	−2.05	−6.40	4.77	−4.17	−21.33	91.46	39.86
28	−6.09	−0.75	14.53	19.61	−13.39	84.00	254.96
29	−4.89	7.60	−14.74	11.01	−5.19	1.49	292.09
30	3.01	3.69	16.87	−5.11	−11.74	26.07	54.03

n_e is the element number, Real (Re), and Imaginary (IM.)

components of the near-field due to the dipoles compared to those obtained by MoM solution are shown in Figure 8(a). It is seen that a good agreement is achieved. The IWO convergence curve is shown in Figure 8(b). The optimization process takes about 18 hours on an Intel (R) core$^{\text{TM}}$ i3 CPU (2.4 GHz) machine. This would have been reduced by 6 hours if we stopped the optimization at 2000 iterations. Although this CPU time might appear to be excessive, the full wave analysis based on MoM for an array of LCRs may take much longer for the direct computations of all the required frequencies. However, the dipoles model can easily be tabulated and used over and over for even other array configurations and by others researcher for other purposes.

3.3. Time-domain Results

The electric and magnetic field radiated by a small dipole in the near field region can be expressed as [26, 43]:

$$\vec{E}=\frac{Z_0 l}{4\pi c}\left[\frac{1}{r}\frac{dI}{dt}\frac{\vec{r}\times\left(\vec{r}\times\vec{l}\right)}{l\cdot r^2}+\left(\frac{c}{r^2}I+\frac{c^2}{r^3}\int I dt\right)\cdot\left(\frac{3\left(\vec{l}\cdot\vec{r}\right)\cdot\vec{r}}{l\cdot r^2}-\frac{\vec{l}}{l}\right)\right] \quad (4)$$

$$\vec{H}=\frac{l}{4\pi c}\left(\frac{1}{r}\frac{dI}{dt}+\frac{c}{r^2}I\right)\frac{\left(\vec{l}\times\vec{r}\right)}{(l\cdot r)} \quad (5)$$

where I is the radiator current, l the dipole length, Z_0 the wave impedance of the free space, c the velocity of light, and r the radius vector to the observation point. Although the time domain Equations (4) and (5) can be used to obtain the near field or the far field pattern of the dipole set, the frequency domain solution of the problem is used and converted to the time domain using the inverse Fourier transform. In other words, by knowing the frequency response of the LCR, which is the summation of electric or magnetic fields of all the dipoles, and the frequency components of the Gaussian pulse, the output radiation patterns in the frequency domain are obtained.

In order to show the efficiency and accuracy of infinitesimal dipole modeling, the same time-domain analysis presented in Section 2 is applied to the obtained infinitesimal dipole set. In other words, the infinitesimal dipole set is excited by the same Gaussian pulse ($\sigma = 2e^{-10}$). The radiated near field patterns of the LCR obtained by using IDMs and MoM solution at a time instance of $t = 1.2/c$ and a distance of $r = 1.2$ m from the antenna aperture are shown in Figure 9. It can be seen that a good agreement is achieved. Therefore, by replacing the antenna with IDM, a very fast and efficient method to model the antenna is achieved. In other words, instead of solving the

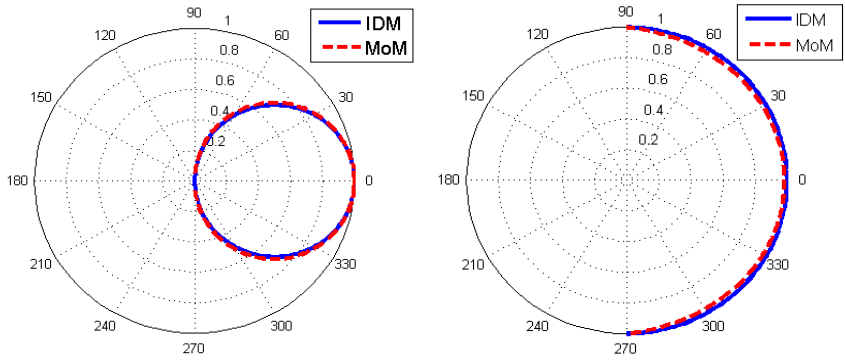

Figure 9. Comparison between the near field patterns of an LCR obtained using the MoM and the IDM excited by a Gaussian pulse at a time instance of $t = 1.2/c$ and a distance of $r = 1.2\,\text{m}$ from the antenna aperture in the (a) E-plane and (b) H-plane.

Table 2. Comparison between the MoM and IDM computational time.

Modeling Method	Computational Time (Sec)
MoM	781
IDM	1.12

LCR by using a full wave method, we replace it with a set of dipoles. A comparison between the time of computing the radiation patterns of the presented antenna by using MoM and IDM is shown in Table 2.

3.4. Elements Coupling

In order to evaluate the validity and efficiency of this method, a 2×2 LCR array is designed and modeled using both the MoM and the IDM methods. This array antenna, having an element spacing of 0.3 m, is solved by full wave MoM software and the IDM method. The same Gaussian pulse presented in the previous section is used to excite each LCR element. A comparison between the time-domain near field patterns of the array at a time instance of $t = 1.2/c$ and a distance of $r = 1.2\,\text{m}$ from the antenna, which are obtained by MoM and IDM, is shown in Figure 10. It can be seen that a good agreement is achieved. Modeling the coupling between the elements using IDMs has been taken into account with the use of the reaction theorem according to [43].

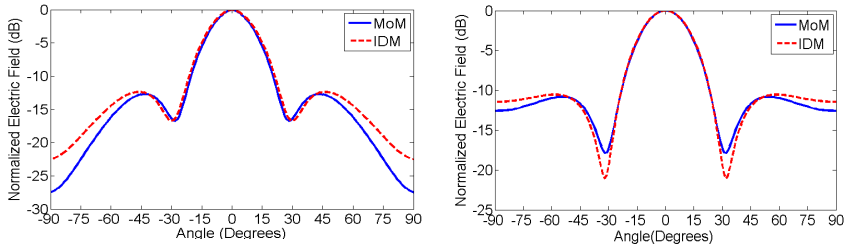

Figure 10. Comparison between the near field patterns of the 2 by 2 antenna array obtained using the MoM and the IDM at a time instance of $t = 1.2/c$ at the distance of $r = 1.2\,\mathrm{m}$ from the antenna, in the (a) E-plane and (b) H-plane.

4. UNIFORMLY SPACED FOCUSED ARRAYS

4.1. 4×4 LCR Array

A two-dimensional square array composed of 16 (4×4) elements, shown in Figure 11, is considered. The array elements are uniformly spaced in the xz-plane with a separation of $d = 0.3\,\mathrm{m}$ between elements. Each LCR element, replaced by a set of dipoles, is excited by the same Gaussian pulse. Therefore, there is an equally weighted amplitude distribution for the array. The array antenna can focus the radiated pulses by setting a proper delay time at each element. Therefore, the radiating waves arrive simultaneously and add up in phase at the desired focusing point. For a focusing distance F from the antenna

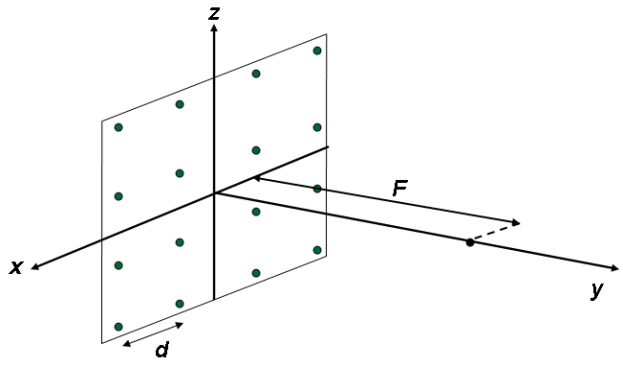

Figure 11. Geometry of uniformly spaced two-dimensional array antenna.

aperture the time delay of i-th element should be set up as

$$t_i = \frac{\sqrt{F^2 + L_i^2}}{c} \tag{6}$$

where c is the speed of light and L_i the distance of the i-th element from the center of the square aperture. The radiation near field pattern of the array at the focal distance from the aperture at time t can be obtained by the summation of the radiated fields of all elements. However, the coupling between the elements is included by using the IDM technique. Figure 12(a) shows the three-dimensional normalized focused beam pattern at the time instance of $t = F/c$ and the focal plane of $F = 1.2\,\mathrm{m}$ of the antenna array. The two-dimensional near field pattern at the time instance of $t = F/c$ and the focal plane, F, is shown in Figure 12(b). It can be seen that moderate sidelobe levels are achieved since no tapering is applied. The near field pattern versus the axial length of the antenna array at the same time instance

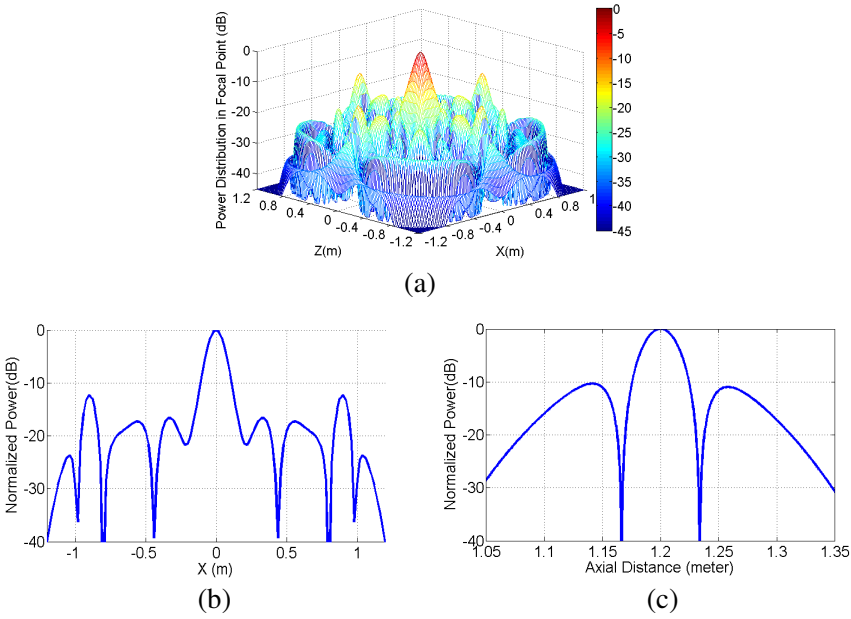

Figure 12. 4 by 4 uniformly spaced array antenna. (a) 3D near field pattern at the time instance of $t = F/c$ and the focal plane ($F = 1.2\,\mathrm{m}$). (b) 2D near field pattern at the time instance of $t = F/c$ and the focal plane ($F = 1.2\,\mathrm{m}$). (c) The normalized field distribution versus the axial distance at the time instance of $t = F/c$.

is illustrated in Figure 12(c). It seems that the maximum intensity occurs at the focal point of the antenna. However, observing the field variations at several different time instances (Figure 13(a)), we can see that a higher intensity value occurs at a point closer to the antenna aperture compared to the focal point. The bold line in Figure 13(a) shows the field at the time instance $t = 1.2\,\mathrm{m/c}$. The variation of peak power values for different time instances are shown in Figure 13(b). It can be seen that the maximum intensity occurs at a point closer to the antenna aperture.

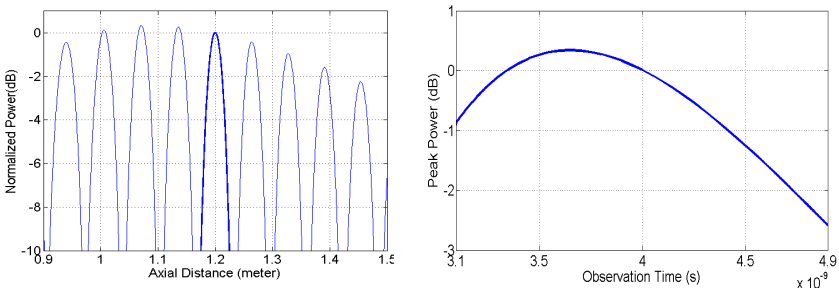

Figure 13. 4×4 uniformly spaced array (a) normalized field distribution versus the axial distance at different time instances. The bold line shows the field at the time instance $t = F/c = 4\,(\mathrm{ns})$. (b) The variation of peak power values for different time instances.

4.2. 8×8 LCR Array

In this section, a larger array antenna composed of 64 (8×8) elements is considered. The elements are separated by $d = 0.3\,\mathrm{m}$, and a Gaussian pulse excites each element. The antenna is designed to have a focal length of 2.4 m. Figure 14(a) shows the three-dimensional normalized focused beam pattern at the focal plane of the antenna array. The two dimensional field pattern of the antenna at the focal plane is shown in Figure 14(b). It can be seen that lower sidelobe levels are achieved for the larger array. Figure 14(c) shows the variation of the near field pattern versus the axial length of the antenna at the time instance of $t = F/c$.

Calculating the near field pattern versus the axial length at different time instances, one can see that the maximum intensity occurs at $y = 2.35\,\mathrm{m}$ from the antenna aperture (Figure 15(a)). The bold line in this figure shows the field at the time instance $t = F/c$. The variation

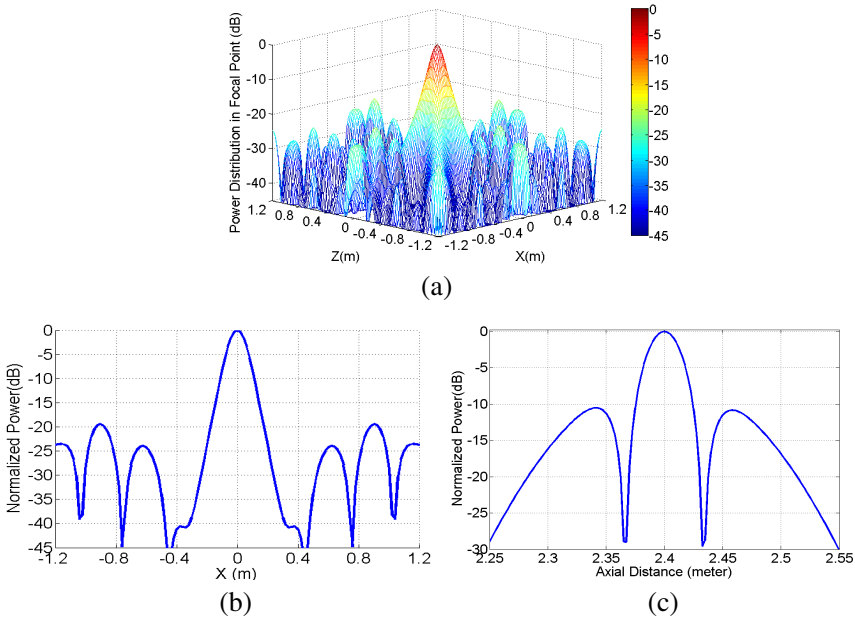

Figure 14. 8×8 array antenna with focal length of 2.4 (m). (a) 3D normalized power pattern at the time instance $t = F/c$ and focal plane. (b) Normalized power pattern at the time instance $t = F/c$ and focal (c) variation of the normalized power pattern versus the axial distance at the time instance of $t = F/c$.

of the peak power for different instances illustrated in Figure 15(b) shows the focal shift in the field pattern of the array antenna.

In the next example, the same 8×8 array antenna is considered with a focal length of 4.8 m. Figure 16(a) shows the variation of the normalized power versus the axial distance at the $t = F/c$ instance. The variation of the power distribution versus the axial distance for different time instances is shown in Figure 16(b). The bold line shows the field at the time instance $t = F/c$. It can be seen that the maximum intensity occurs at $y = 4.48$ m from the antenna aperture. The variation of the peak power versus the different time instances for the 8×8 array is shown in Figure 16(c). It can be seen that by increasing the focal length the focal shift has been increased. In order to further study the behavior of the focal shift, the 8×8 array antenna with many different focal lengths is modeled. Table 3 depicts the variations of the maximum intensity length and the difference between the power values at the focal point and maximum intensity point for

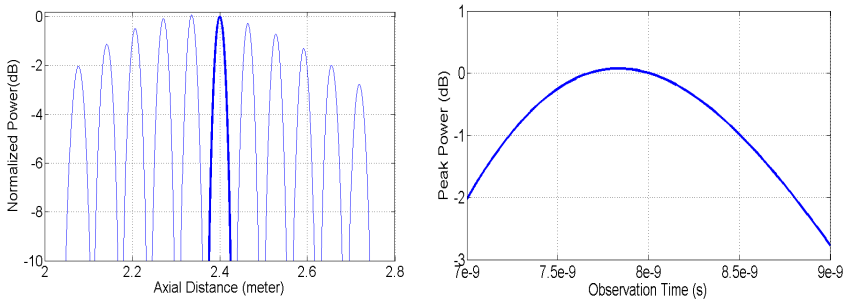

Figure 15. The 8 by 8 array with $F = 2.4\,\text{m}$. (a) The variation of the near field pattern versus the axial length at different time instances. The bold line shows the field at the time instance $t = F/c = 8\,(\text{ns})$. (b) The variation of the peak power at different time instances.

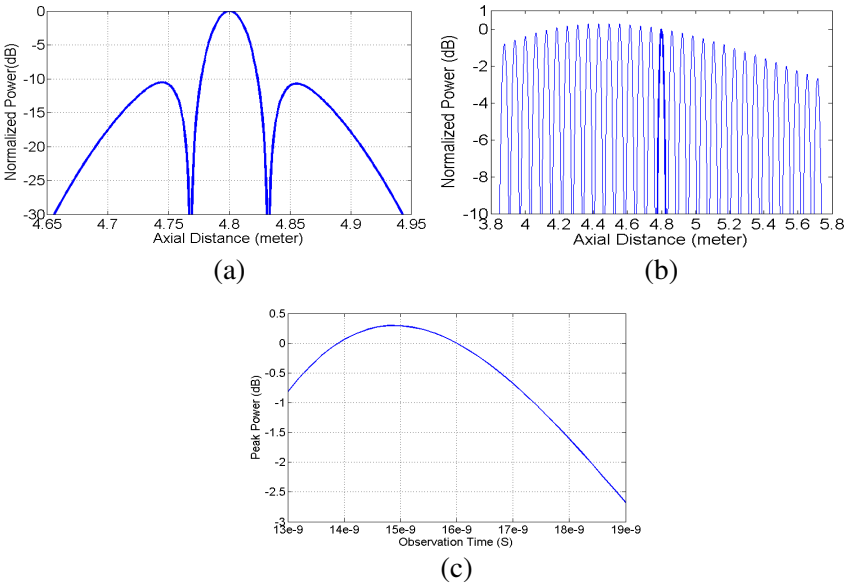

Figure 16. The 8×8 array antenna with $F = 4.8\,\text{m}$. (a) The variation of the normalized power pattern versus the axial distance. (b) The variation of the near field pattern versus the axial length at different time instances. The bold line shows the field at the time instance $t = F/c = 16\,(\text{ns})$. (c) The variation of the peak power versus the different time instances at the focal point.

Table 3. Focusing properties of the 8×8 array at different focal lengths.

Focal length (m)	1.2	2.4	3.6	4.8	6	7.2	8.4	9.6
Maximum Intensity position (m)	1.18	2.35	3.44	4.48	5.39	6.21	6.96	7.6
Peak Power Difference (dB)	0.005	0.074	0.17	0.30	0.46	0.60	0.86	1.04

different focal lengths of the 8 by 8 array antenna. It can be seen that similar to narrow band antennas, for the focal point close to the antenna aperture, the maximum intensity is very close to the focal point, but as the focal point moves away from the antenna aperture, the focal shift increases. In addition, by increasing the focal length, the difference between the peaks at maximum intensity point and focal point is increased.

5. CONCLUSIONS

Some focusing properties of the ultra-wideband time-domain focused array antennas were presented. Large current radiators are considered as the elements of the antenna array. In order to model the large array antenna while the mutual coupling between the elements is taken into account, each LCR element is replaced with a set of infinitesimal dipoles generating the same near field pattern as the actual element. Using this technique a fast and accurate simulation tool was achieved.

Calculating the variation of the power distributions versus the axial length at different time instances showed the focal shift effect in the near-field pattern. It was shown that the maximum intensity occurred at a point closer to the antenna aperture than the focal distance and this displacement was increased as the focal point moved away from the antenna aperture. It was shown that this displacement can only be seen when the radiated pulse is observed at successive time instants.

REFERENCES

1. Sherman, J. W., "Properties of focused aperture in the Fresnel region," *IRE Trans. on Antennas Propagat.*, Vol. 10, No. 4, 399–408, 1962.

2. Hanson, R. C., "Focal region characteristics of focused array antennas," *IEEE Trans. on Antennas and Propagat.*, Vol. 33, No. 6, 1328–1337, 1985.
3. Graham, W. J., "Analysis and synthesis of axial field patterns of focused apertures," *IEEE Trans. on Antennas and Propagat.*, Vol. 31, No. 4, 665–668, 1983.
4. Karimkashi, S. and A. A. Kishk, "A new Fresnel zone antenna with beam focused in the Fresnel region," *URSI National Radio Science Meeting*, Chicago, 2008.
5. Karimkashi, S. and A. A. Kishk, "Focused microstrip array antenna using a Dolph-Chebyshev near-field design," *IEEE Trans. on Antennas and Propagat.*, Vol. 57, No. 12, No. 12, 3813–3820, Dec. 2009.
6. Karimkashi, S. and A. A. Kishk, "Focusing properties of Fresnel zone plate lens antennas in the near-field region," *IEEE Trans. on Antennas and Propagat.*, Vol. 59, No. 5, 1481–1487, May 2011.
7. Karimkashi, S. and J. Rashed-Mohassel, "Blockage minimization in symmetric dual reflector antennas for different edge taper values," *Journal of Electromagnetic Waves and Applications*, Vol. 20, No. 4, 505–514, 2006.
8. Sirenko, K., V. Pazynin, Y. K. Sirenko, and H. Bagci, "Compression and radiation of high-power short RF Pulses. II. A novel antenna array design with combined compressor/radiator elements," *Progress In Electromagnetics Research*, Vol. 116, 271–296, 2011.
9. Hackett, D. R., C. D. Taylor, D. Mclemore, H. Dogliani, W. A. Walton, and A. J. Leyendecker, "A transient array to increase the peak power delivered to a localized region in space: Part I — Theory and modeling," *IEEE Trans. on Antennas and Propagat.*, Vol. 50, No. 12, 1743–1750, Dec. 2002.
10. Jacobsen, S., "Reduction of hot spots in hyperthermia by means of broadband energy transmission," *Electron. Lett.*, Vol. 34, No. 20, 1901–1902, Oct. 1998.
11. Converse, M. C., E. J. Bond, S. C. Hagness, and B. D. Van Veen, "Ultrawide-band microwave space-time beamforming for hyperthermia treatment of breast cancer: A computational feasibility study," *IEEE Trans. on Microw. Theory and Tech.*, Vol. 52, No. 8, 1876–1889, Aug. 2004.
12. Converse, M., E. J. Bond, B. D. Van Veen, and S. Hagness, "A computational study of ultra-wideband versus narrowband microwave hyperthermia for breast cancer treatment," *IEEE Trans. on Microw. Theory and Tech.*, Vol. 54, No. 5, 2169–2180,

May 2006.

13. Baum, C. E., et al., "Transient arrays," *Ultra-wideband, Short-pulse Electromagnetics 3*, 129–138, New York, Plenum, 1997.
14. Hussain, M. G. M., "Characteristics of ultra-wideband electromagnetic missiles generated by focused two-dimensional array," *Progress In Electromagnetics Research*, Vol. 49, 143–159, 2004.
15. Schwartz, J. L. and B. D. Steinberg, "Properties of ultrawideband arrays," *Ultra-wideband, Short-pulse Electromagnetics 3*, 139–145, New York, Plenum, 1997.
16. Durney, C. H. and M. F. Iskandar, "Antennas for medical applications," *Antenna Hand Book: Theory, Applications, and Design*, Ch. 24, New York, Van Nostrand, 1988.
17. Baum, C. E., *Focused Aperture Antennas, Air Force Research Laboratory*, Kirtland AFB, NM, 1987.
18. Kang, Y. W. and D. M. Pozar, "Optimization of pulse radiation from dipole arrays for maximum energy in a specified time interval," *IEEE Trans. on Antennas and Propagat.*, Vol. 34, 1383–1390, Dec. 1986.
19. Taylor, J. D. (ed.), *Introduction to Ultra-wideband Radar Systems*, CRC, Boca Raton, FL, 1995.
20. Hussain, M. G. M., "Ultra-wideband impulse radar — An overview of the principles," *IEEE Aerosp. Electron. Syst. Mag.*, Vol. 31, No. 9, 9–14, Sep. 1998.
21. Di Benedetto, M., et al., *UWB Communication Systems: A Comprehensive Overview*, Hindawi, New York, 2006.
22. Gresham, I., et al, "Ultra-wideband radar sensors for short-range vehicular applications," *IEEE Trans. on Microw. Theory and Tech.*, Vol. 52, No. 9, 2105–2122, 2004.
23. Hussain, M. G. M., "Antenna patterns of nonsinusoidal waves with the time variation of a Gaussian pulse: Parts I and II," *IEEE Trans. on Electromag. Compat.*, Vol. 3, No. 4, 504–522, Nov. 1988.
24. Ziolkowski, R. W., "Properties of electromagnetic beams generated by ultra-wide bandwidth pulse-driven arrays," *IEEE Trans. on Antennas and Propagat.*, Vol. 40, No. 8, 888–905, Aug. 1992.
25. Hussain, M. G. M., "Principles of space-time array processing for ultrawide-band impulse radar and radio communications," *IEEE Trans. on Veh. Technol.*, Vol. 51, No. 3, 393–403, May 2002.
26. Shlivinski, A. and E. Heyman, "A unified kinematic theory of transient arrays," *Ultra-wideband, Short-pulse Electromagnetics*, Kluwer Academic/Plenum, New York, 2002.

27. Shlivinski, A., "Kinematic properties of short-pulsed sparse transmitting arrays," *Progress In Electromagnetics Research*, Vol. 115, 11–33, 2011.
28. Hussain, M. G. M. and A. S. Al-Zayed, "Aperture-sparsity analysis of ultrawideband two-dimensional focused array," *IEEE Trans. on Antennas and Propagat.*, Vol. 56, 1908–1918, Jul. 2008.
29. Harmuth, H. F. and N. J. Mohamed, "Large-current radiators," *IEE Proceedings — H*, Vol. 139, No. 4, 358–362, Aug. 1992.
30. Pochanin, G., V. Kholod, and S. A. Masalov, "Large current radiator with S-diode switch," *IEEE Trans. on Electromagn. Compat.*, Vol. 43, No. 1, 94–100, 2001.
31. Pochanin, G. and S. A. Masalov, "Use of the coupling between elements of the vertical antenna array of LCRs to gain radiation efficiency for UWB pulses," *IEEE Trans. on Antennas and Propagat.*, Vol. 55, No. 6, 1754–1759, Jun. 2007.
32. Hussain, M. G. M., *Antenna Pattern of Large-current Radiator and Closed-loop Sensor* Anaheim, California, 1992.
33. Lukin, K. A., G. Pochanin, and S. A. Masalov, "Large current radiator with avalanche transistor Switch," *IEEE Trans. on Electromagn. Compat.*, Vol. 39, No. 2, 156–159, May 1997.
34. Wehr, M. and G. Monich, "Detection of radiation leaks by spherically scanned field data," *Proc. 10th Int. Zurich Symp. Technol. Exhb. EMC*, Zurich, 1993.
35. Wehr, M., A. Podubrin, and G. Monich, "Automated search for models by evolution strategy to characterize radiators," *Proc. 11th Int. Zurich Symp. Technol. Exhb. EMC*, Zurich, 1995.
36. McNay, D., E. Michielssen, R. L. Rogers, S. A. Taylor, M. Akhtari, and W. W. Sutherling, "Multiple source localization using genetic algorithms," *J. Neurosci. Methods*, Vol. 64, 163–172, Feb. 1996.
37. Regue, J.-R., M. Ribo, J.-M. Garrell, and A. Martin, "A genetic algorithm method for source identification and far-field radiated emissions predicted from near-field measurements for PCB characterization," *IEEE Trans. on Electromagn. Compat.*, Vol. 43, 520–530, Nov. 2001.
38. Sijher, T. S. and A. A. Kishk, "Antenna modeling by infinitesimal dipoles using genetic algorithms," *Progress In Electromagnetics Research*, Vol. 52, 225–254, 2005.
39. Mikki, S. M. and A. A. Kishk, "Theory and applications of infinitesimal dipole models for computational electromagnetics," *IEEE Trans. on Antennas and Propagat.*, Vol. 55, 1325–1337, 2007.

40. Wu, X. H., A. A. Kishk, and A. W. Glisson, "A transmission line method to compute the far-field radiation of arbitrary Hertzian dipoles in a multilayer structure embedded with PEC strip interfaces," *IEEE Trans. on Antennas and Propagat.*, Vol. 55, 3191–3198, Nov. 2007.
41. Wu, X. H., A. A. Kishk, and A. W. Glisson, "A transmission line method to compute the far-field radiation of arbitrarily directed Hertzian dipoles in a multilayer dielectric structure: Theory and applications," *IEEE Trans. on Antennas and Propagat.*, Vol. 54, 2731–2741, Oct. 2006.
42. Wu, X. H., A. A. Kishk, and A. W. Glisson, "Modeling of wide band antennas by frequency-dependent Hertzian dipoles," *IEEE Trans. on Antennas and Propagat.*, Vol. 56, 2481–2489, Aug. 2008.
43. Karimkashi, S., A. A. Kishk, and D. Kajfez, "Antenna array optimization using dipole models for MIMO applications," *IEEE Trans. on Antennas and Propagat.*, Vol. 59, No. 8, 3112–3116, 2011.
44. Karimkashi, S., A. A. Kishk, and G. Zhang, "Modelling of aperiodic array antennas using infinitesimal dipoles," *IET Microwaves, Antennas Propagat.*, Vol. 6, No. 7, 761–767, 2012.
45. Richmond, J., "A reaction theorem and its application to antenna impedance calculations," *IRE Trans. on Antennas Propag.*, Vol. 9, No. 6, 515–520, 1961.
46. Harmuth, H. F., *Sequence Theory, Foundations and Applications*, Academic, New York, 1977.
47. Harmuth, H. F., *Nonsinusoidal Waves for Radar and Radio Communication*, Academic, New York, 1981.
48. Harmuth, H. F., *Antennas and Waveguides for Nonsinusoidal Waves*, Academic, New York, 1984.